



ELSEVIER

Magnetic-plasmonic nanoparticles for the life sciences: calculated optical properties of hybrid structures

Ward Brullot, MSc*, Ventsislav K. Valev, PhD, Thierry Verbiest, PhD

Laboratory for Molecular Electronics and Photonics, Department of Chemistry, Katholieke Universiteit Leuven, Belgium

Received 28 June 2011; accepted 7 September 2011

Abstract

Magnetic-plasmonic nanoparticles, combining magnetic and plasmonic components, are promising structures for use in life sciences. Optical properties of core-shell magnetite-gold nanostructures, such as the wavelength of the plasmon resonance, the extinction cross-section, and the ratio of scattering to absorption at the plasmon wavelength are critical parameters in the search for the most suitable particles for envisioned applications. Using Mie theory and the discrete dipole approximation (DDA), optical spectra as a function of composition, size, and shape of core-shell nanospheres and nanorods were calculated. Calculations were done using simulated aqueous media, used throughout the life sciences. Our results indicate that in the advantageous near-infrared region (NIR), although magnetic-plasmonic nanospheres produced by available chemical methods lack the desirable tunability of optical characteristics, magnetic-plasmonic nanorods can achieve the desired optical properties at chemically attainable dimensions. The presented results can aid in the selection of suitable magnetic-plasmonic structures for applications in life sciences.

From the Clinical Editor: In this basic science study, magnetic-plasmonic nanoparticles are studied for future applications in life sciences. Optical properties of core-shell magnetite-gold nanostructures, such as the wavelength of the plasmon resonance, the extinction cross-section, and the ratio of scattering to absorption at the plasmon wavelength are critical parameters in the search for the most suitable particles for proposed future applications.

© 2012 Elsevier Inc. All rights reserved.

Key words: Magnetic-plasmonic nanoparticles; Core-shell nanoparticles; Magnetite-gold; Nanorods; Calculated optical properties

Both plasmonic and magnetic nanomaterials are currently under intensive investigation for use in biomedical applications, and many findings have already been commercially exploited.^{1–4} The field of magnetic-plasmonic nanostructures, in which plasmonic and magnetic materials are combined, however, is only just emerging. Such multifunctional structures are commonly called “theranostic” structures in biomedical contexts due to their therapeutic and diagnostic potentials.^{2,5}

Magnetic nanostructures used in biomedical applications are usually composed of iron oxides, such as magnetite or

maghemite because these materials combine high magnetic susceptibilities with very low toxicity.^{2,6} Spherical iron or iron oxide based nanoparticles (NPs) can be prepared by a variety of well-known synthesis methods. Most methods currently available provide iron oxide nanospheres with an average diameter well below the superparamagnetic limit,⁷ which is about 30 nm for magnetite.⁸ Above the superparamagnetic limit, iron oxide NPs become ferri- or ferromagnetic. Besides spherical or cube-shaped particles, iron oxide nanorods have also been chemically synthesized.^{9,10} For example, Kumar et al,¹⁰ have synthesized 12 x 48 nm magnetite nanorods. If superparamagnetic NPs are surrounded by a suitable coating layer, they can be dispersed in a carrier liquid (e.g., water) and form a stable magnetic fluid or ferrofluid.³ Ferri- or ferromagnetic NPs, i.e., above the superparamagnetic limit, require an extensive stabilizing hydrophilic coating layer in aqueous environments to prevent precipitation due to magnetostatic interactions.¹¹

Biocompatible magnetic particles or fluids can be used as magnetic drug-targeting agents,¹² magnetic resonance imaging (MRI) contrast agents,² and as an agent for localized AC magnetic field hyperthermia.³ Another interesting application is

W. Brullot received funding from the Agency for Innovation by Science and Technology (IWT) Flanders (Research funded by a PhD grant of the Agency for Innovation by Science and Technology (IWT)), V.K. Valev received funding from the Fund for Scientific Research Flanders (FWO-Vlaanderen). T. Verbiest received GOA funding from the Katholieke Universiteit Leuven.

*Corresponding author: Laboratory for Molecular Electronics and Photonics, Department of Chemistry, Katholieke Universiteit Leuven, Celestijnenlaan 200D, 3001 Heverlee (Leuven), Belgium.

E-mail addresses: ward.brullot@fys.kuleuven.be, ward.brullot@gmail.com (W. Brullot).

magnetic separation of species in solution using magnetic NPs conjugated with a specific binding agent.¹³

Plasmonic NPs, i.e., NPs exhibiting localized surface plasmon resonances, can show strong optical resonances for visible and near-infrared wavelengths.^{1,14,15} This is due to the collective oscillations of free conduction electrons when illuminated with light at the plasmon wavelength (λ_{\max}). For metallic NPs, e.g. gold and silver,^{14,15} this resonance mode is called a localized surface plasmon resonance (LSPR). Plasmon resonances endow nanostructures with unique optical properties, such as strongly enhanced absorption and scattering at the plasmon resonance wavelength. The intensity and position of the plasmon resonance heavily depend on the size and shape of the plasmonic structure and the surrounding medium.

Plasmonic particles show efficient heating at λ_{\max} due to the strongly enhanced absorption,¹⁶ which is exploited in medical cancer therapies such as photothermal therapy^{1,17,18} or heat-induced release of antitumor drugs.¹⁹ Plasmonic heating is also used in diagnostic techniques such as photoacoustic²⁰ or photothermal imaging.¹⁶ The superior scattering efficiencies of plasmonic nanostructures have been used in biomedical contexts for optical biosensors²¹ and contrast agents for imaging in, for example, optical coherence tomography.²²

The position of the plasmon band is of great importance for biomedical applications. Hemoglobin and water, the dominant contributors to the absorption spectrum of living tissue, show a minimum in their absorption spectra in the NIR of the spectrum (650 nm – 900 nm).^{23,24} As such, the NIR is the preferred region to position λ_{\max} for optical biomedical applications. Structures consisting of a dielectric core surrounded by a plasmonic shell, like silica-gold core-shell nanospheres, show redshifted plasmon bands and have recently been used as NIR photothermal probes.^{1,15}

Gold is predominantly used as plasmonic metal for biomedical applications because of its biocompatibility, well-defined synthesis routes, resistance to oxidation, and flexible conjugation possibilities with organic molecules.^{4,16,22}

Magnetic-plasmonic nanostructures are integrated magnetic and plasmonic materials. Although the individual materials already allow many applications, integrated nanostructures greatly extend the possibilities. Figure 1 shows the relevant processes in such hybrid nanostructures. Incident photons can be scattered or absorbed, generating plasmon bands, heat, or scattering contrast. External magnetic fields can be used to generate heat through conversion of AC magnetic field energy losses, facilitate guidance of particles, and generate extra contrast in MRI.

Such multimodal structures have a very broad applicability. Some examples are the use of magnetic-plasmonic nanostructures for MRI and photothermal therapy²⁵ or for simultaneous MRI and drug release.²⁶ Other possibilities include following DC magnetic field guided magnetic-plasmonic particles by scattering imaging, combining magnetic separation in solution with plasmonic detection methods, or concomitant magnetic hyperthermia and photothermal therapy for cancer treatment.

In many, if not all, envisioned applications, the position and strength of the LSPR response of the integrated nanostructures is of great importance. The optical properties of homogeneous

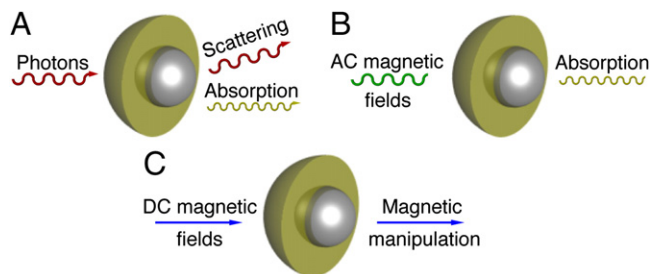


Figure 1. Overview of relevant processes in hybrid magnetic-plasmonic nanoparticles composed of a magnetic core and a plasmonic shell. (A) scattering or absorption of photons; (B) absorption of AC magnetic field energy; (C) use of DC magnetic fields to magnetically manipulate the nanostructures.

and core-shell nanospheres and nanorods have already been assessed theoretically and experimentally.^{14,15,17,27–29} Experimentally, magnetite-gold core-shell spherical NPs have been produced,^{30–35} but to our best knowledge, none with a magnetite core larger than the superparamagnetic limit. Although hybrid structures have been synthesized, no theoretical framework for the rational design of magnetic-plasmonic nanostructures for life science applications, based on optical characteristics, has been reported yet.

Important to note is that besides the separate magnetic and plasmonic properties of hybrid structures taken into account in current work, interplay, called magnetoplasmonics, exists between both components. A prominent example of this interplay is enhancement of magneto-optical effects through plasmon excitation.^{33,36,37} For nanostructures such as those studied in this work, such magnetoplasmonic effects generally influence only the polarization state of the optical beam while passing through the sample.³⁸ The polarization state of light is only important for the rodlike shapes, because they are anisotropic, and as NPs in tissue generally rotate, the polarization state of the used light is of minor importance for biomedical applications. Therefore, magnetoplasmonic effects are not taken into account in current work.

In this work, optical properties such as λ_{\max} , the extinction cross-section ($C_{\text{extinction}}$), and the ratio of scattering to absorption cross-sections ($C_{\text{scattering}}/C_{\text{absorption}}$) at λ_{\max} of magnetic-plasmonic magnetite-gold nanostructures were calculated. The influence of nanostructure composition, size, and shape on these optical properties was investigated. Furthermore, the optical characteristics of magnetic-plasmonic nanostructures were quantitatively compared with those of organic dyes applied in biomedical environments.

For core-shell spheres, calculations were performed using the analytically correct Mie theory for multilayered spherical structures.^{14,15,39} Calculating optical spectra for nanostructures with an arbitrary geometry can be done with several numerical techniques, such as the multiple multipole,⁴⁰ the finite difference time domain method²⁹ or the DDA method. The DDA method was chosen to calculate the optical spectra of nanorod structures because it has proven to be a powerful technique for calculating optical characteristics of structures with an arbitrary geometry in a dielectric environment.^{14,15}

Magnetite and gold were respectively chosen as magnetic and plasmonic material for the performed calculations because both materials have been intensively studied. Magnetite is a very well-known material possessing the highest saturation magnetization of all iron oxides,⁶ and gold is the predominantly used plasmonic material in biosciences.

The findings and insights can aid in the rational design of magnetic-plasmonic nanostructures with applications in the life sciences.

Calculation method

Extinction, scattering, and absorption efficiencies ($Q_{\text{extinction}}$, $Q_{\text{scattering}}$ and $Q_{\text{absorption}}$) as a function of wavelength for core-shell nanospheres were calculated using Mie theory for spherical. Calculations were performed using MieLab.³⁹ Input parameters were the thickness of each layer in the spherical nanostructure, R_i , the complex dielectric functions, ϵ_i , and the complex refractive index of the medium. This last parameter was chosen to be that of water, $1.33 + 0i$, because many environments encountered in biomedical applications, such as blood or perfused tissues, can be approximated as aqueous environments. To improve comparability with previous seminal work,^{15,17} bulk dielectric functions of materials were used.^{41,42} Corrections for size are generally calculated via the damping constant, which has an effect only as a possible line broadening mechanism.⁴³ Furthermore, because most of the calculated structures are above the size limit for corrections, the influence of not correcting for size on the predicted trends and values are minimal.

The dimensions of core-shell nanospherical structures cannot be represented by a single radius but are defined by the total radius for the structure (R_{total}) as the sum of the radii of the magnetic core (R_{core}) and the surrounding dielectric shell (R_{shell}). Optical properties of core-shell nanospheres were calculated for two sets of structures. One has a fixed R_{total} and varying R_{core} , and a second has a fixed $R_{\text{core}}/R_{\text{total}}$ ratio while varying R_{total} . As such, the influence of the two defining structural parameters, size and core-shell ratio, on the optical properties was investigated.

Optical characteristics of magnetic-plasmonic nanorods were calculated using the DDA method.^{44,45} Nanorods were modeled as cylinders with hemispherical end caps,²⁷ and the aspect ratio was defined as the ratio of the total length of the rod, including the hemispherical end caps, to the maximal diameter.

To represent the size of nanorod structure, an effective radius ($R_{\text{effective}}$) was defined. This $R_{\text{effective}}$ is equal to the radius of a sphere that possesses the same volume as that of the nanorod. To describe the core-shell nature of the calculated nanorod structures, the $V_{\text{core}}/V_{\text{total}}$ ratio is used. As such, nanorods can be structurally described by their aspect ratio, the effective radius and the $V_{\text{core}}/V_{\text{total}}$ ratio.

Calculations were performed for a fixed orientation of the nanorods whereby the propagation of the incident light wave is perpendicular to the long axis of the structure. This was done to ensure excitation of the longitudinal dipolar localized surface plasmon resonance. Two orthogonal polarizations of the incoming light were used, one with the electric field

perpendicular and the other parallel to the long axis of the nanorod.

From the calculated spectra of the $Q_{\text{extinction}}$, $Q_{\text{scattering}}$ and $Q_{\text{absorption}}$ efficiencies, λ_{max} can be obtained. The corresponding extinction, scattering, and absorption cross-sections ($C_{\text{extinction}}$, $C_{\text{scattering}}$, and $C_{\text{absorption}}$) can be obtained by multiplying the calculated efficiencies with the geometrical cross-sectional area of the structures in the incoming light. These cross-sections represent a geometrical area of a particle that contributes to the extinction, absorption, or scattering and can be directly related to molar coefficients used in spectroscopy. Knowing the absolute values of the calculated cross-sections, it is possible to calculate $C_{\text{scattering}}/C_{\text{absorption}}$ at λ_{max} , which is an important parameter when selecting particles for applications. This parameter indicates the relative degree with which a structure scatters or absorbs light and is a key factor in choosing the suitable structure for the foreseen application. For some applications, scattering of light is the main process, as in, for example, resonance scattering imaging, whereas others require a high absorption coefficient, such as photothermal therapy. The first application requires a high and the second a low $C_{\text{scattering}}/C_{\text{absorption}}$ ratio.

As stated earlier, the calculated cross-sections (in cm^2) can be converted to molar coefficients (in $\text{L mol}^{-1} \text{cm}^{-1}$) used in spectroscopy. The formula used is,⁴⁶

$$\epsilon = \frac{C_i N_A}{10001n(10)} = \frac{C_i}{3.82 \times 10^{-21}} \quad \text{Equation 1}$$

in which ϵ represents the molar coefficient, C_i the relevant cross-section and N_A the Avogadro constant. As molar coefficients are known for many organic dyes used in biomedical applications, a useful comparison between these dyes and magnetic-plasmonic nanostructures becomes possible.

Results

As stated in the Calculation method section, three important optical parameters were obtained from the calculated $Q_{\text{extinction}}$, $Q_{\text{scattering}}$ and $Q_{\text{absorption}}$ spectra. These were λ_{max} , the corresponding cross-sections ($C_{\text{extinction}}$, $C_{\text{scattering}}$ and $C_{\text{absorption}}$), and $C_{\text{scattering}}/C_{\text{absorption}}$ at λ_{max} . It is important to note that these parameters are not independent. Because the dielectric functions of the materials change throughout the spectrum, the cross-sections and their ratio at λ_{max} also change when shifting λ_{max} .

The general influence of the structural parameters of core-shell nanospheres and nanorods, i.e., size, core-shell ratio, and shape, on the optical characteristics can be rationalized. Keeping all other parameters constant, increasing size is expected to cause a redshift of λ_{max} due to the electromagnetic retardation effect³³ and an increase in $C_{\text{extinction}}$ at λ_{max} due to the extra amount of contributing material present in a single particle. The influence of size on the $C_{\text{scattering}}/C_{\text{absorption}}$ ratio at λ_{max} depends on the dielectric functions of the constituting materials at the shifted λ_{max} and also on the size- and wavelength-dependent Rayleigh scattering.

Increasing the core-shell ratio, i.e., coating the particles with a thinner metallic shell generally results in a redshift of λ_{max} . This

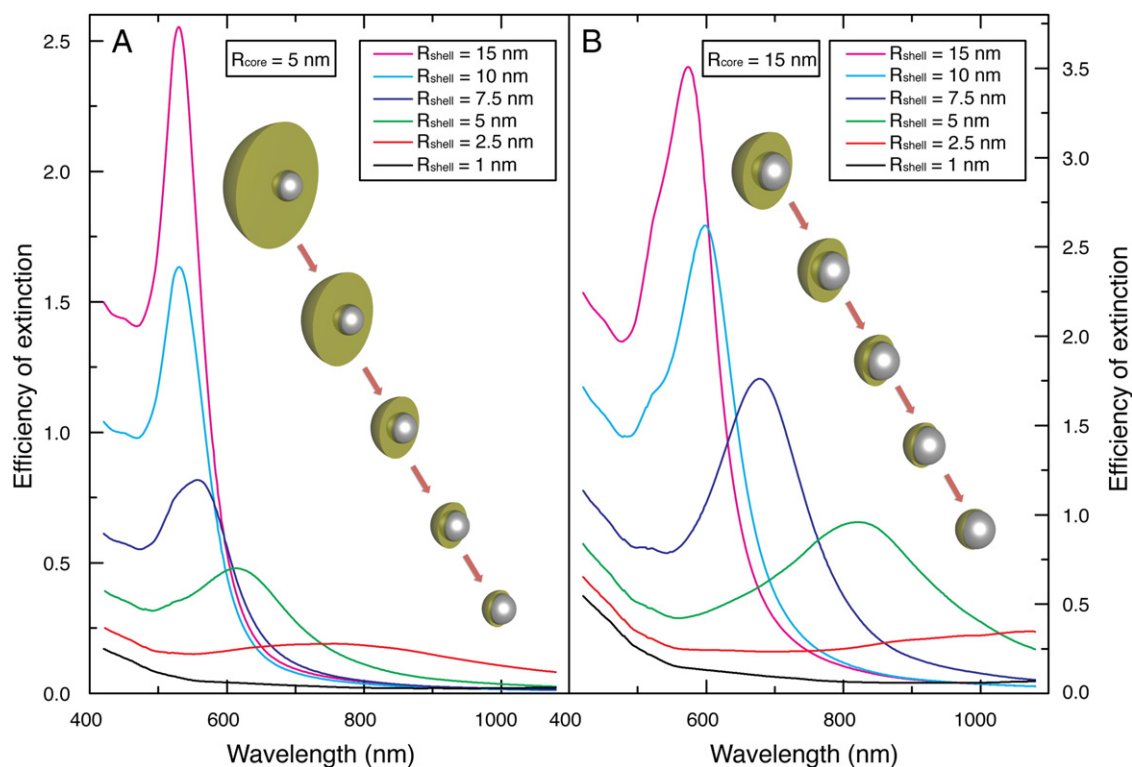


Figure 2. $Q_{\text{extinction}}$ as a function of wavelength for core-shell nanospheres with (A) an R_{core} of 5 nm or (B) an R_{core} of 15 nm and an increasing gold shell thickness (R_{shell}). The spectra show redshifts of λ_{max} and decreasing $Q_{\text{extinction}}$ at λ_{max} with decreasing shell thickness.

response can be explained by considering the inside and outside of the gold shell as separate species, generating plasmon modes that couple across the shell to result in the observable optical spectra. As such, thinner shells facilitate coupling of the plasmon modes, resulting in a redshift of λ_{max} .²⁸ A large core-shell ratio also causes a decrease in $C_{\text{extinction}}$ at λ_{max} due to a lower amount of plasmonic metal per particle. As for the size parameter, the influence of the core-shell ratio on the $C_{\text{scattering}}/C_{\text{absorption}}$ at λ_{max} depends on the dielectric functions of the materials at the shifted λ_{max} .

The *aspect ratio* is a third variable parameter for magnetic-plasmonic nanorods. Increasing the aspect ratio is expected to cause a redshifted λ_{max} for the longitudinal plasmon band due to the increased path length for electron oscillation along the long axis.⁴⁷ Furthermore, increasing the aspect ratio is likely to result in a larger $C_{\text{extinction}}$ at λ_{max} . This larger $C_{\text{extinction}}$ can be attributed to enhanced coupling between the inner and outer plasmon modes of the plasmonic shell of core-shell structures with a higher aspect ratio.⁴⁷

In the following paragraphs, results of calculations on core-shell magnetite-gold nanospheres and nanorods will be discussed. The general considerations described in the earlier paragraphs will be of great help when rationalizing the obtained results.

Magnetic-plasmonic nanospheres

As stated earlier, available chemical synthesis routes mostly provide magnetite cores with an average radius of 5 nm, whereas

the superparamagnetic limit for such structures is approximately 15 nm. Calculated optical properties for core-shell nanospheres with an R_{core} of 5 nm or 15 nm and increasingly thinner gold shells are shown in Figure 2. These spectra indicate the shift of λ_{max} by simultaneously changing the composition and size of the core-shell nanospheres.

As expected, calculations showed that a thinner shell exhibits a greater redshift in comparison with a thicker shell and shows a lower $Q_{\text{extinction}}$ due to a decrease in the amount of gold per particle. The calculated results are consistent with experimentally obtained results for similar systems.^{32–35} From Figure 2, A it is evident that coating magnetite particles with an R_{core} of 5 nm with a gold shell does not provide efficient tuning of the plasmon band, nor high $Q_{\text{extinction}}$ throughout the NIR. As can be seen from Figure 2, B, coating particles with a size around the superparamagnetic limit with a gold shell reveals two compositions, with a 5 nm and a 7.5 nm gold shell, to show plasmon bands in the advantageous NIR. These results indicate a trend in which magnetic-plasmonic nanospheres consisting of larger cores show higher tunabilities in the NIR. Furthermore, small spherical NPs as calculated here, exhibit very small $C_{\text{scattering}}/C_{\text{absorption}}$ at λ_{max} due to the size and wavelength dependence of Rayleigh scattering. This diminishes their applicability in scattering applications.

Despite that core-shell magnetite-gold nanospheres larger than the superparamagnetic limit have, to our best knowledge, not been experimentally synthesized yet, optical characteristics as a function of structural parameters for such nanostructures were calculated. This provides deeper insight into the trends of

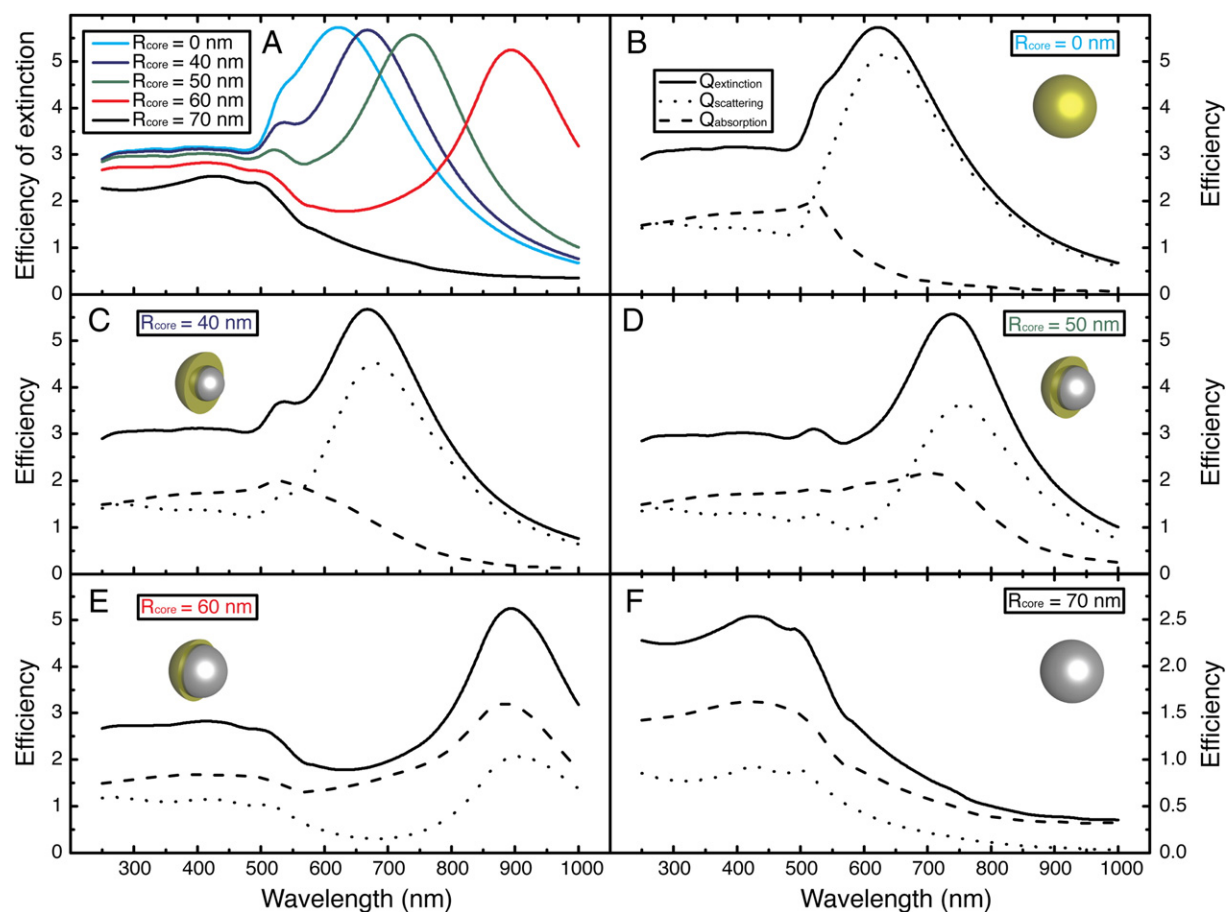


Figure 3. Calculated optical properties of core-shell nanospheres for a fixed R_{total} of 70 nm; (A) $Q_{\text{extinction}}$ for all calculated R_{core} ; (B–F) $Q_{\text{extinction}}$ (solid line), $Q_{\text{scattering}}$ (dotted line) and $Q_{\text{absorption}}$ (dashed line) for R_{core} equal to 70 nm, 60 nm, 50 nm, 40 nm, and 0 nm. The spectra indicate the shifts of λ_{max} and changes in $Q_{\text{extinction}}$ and contributions of $Q_{\text{scattering}}$ and $Q_{\text{absorption}}$ with altering magnetic-plasmonic nanosphere composition.

optical properties indicated by the results described in the previous paragraph.

Calculated optical spectra for core-shell nanospheres with a fixed R_{total} of 70 nm and a varying R_{core} of 70, 60, 50, 40, and 0 nm are shown in Figure 3, A. The calculated plasmon peaks are located in the advantageous NIR of the spectrum. As for the smaller core-shell nanospheres calculated earlier, structures with an increasingly thinner gold shell show an increasingly more redshifted λ_{max} . Although a slight decrease of the maximum $Q_{\text{extinction}}$ can be observed for a decreasing volume of gold, high efficiencies are calculated for all studied core-shell nanospheres. Besides the dipolar plasmon band, another resonant peak can be observed at a shorter wavelength. The existence of this band can be attributed to quadrupolar interactions in the dielectric shell.¹⁵

Figures 3, B–F show the calculated spectra of $Q_{\text{extinction}}$, $Q_{\text{scattering}}$, and $Q_{\text{absorption}}$ of core-shell nanospherical structures with fixed R_{total} of 70 nm and stepwise increasing R_{core} . From the graphs it is apparent that not only λ_{max} shifts but also that the relative contributions of scattering and absorption drastically change with altering core-shell composition.

In Figure 4, the dependencies of λ_{max} , $C_{\text{extinction}}$ and $C_{\text{scattering}}/C_{\text{absorption}}$ at λ_{max} on the $R_{\text{core}}/R_{\text{total}}$ ratio with fixed R_{total} and on R_{total} with fixed $R_{\text{core}}/R_{\text{total}}$ are plotted. In the first

case R_{total} is fixed to 70 nm and in the second case $R_{\text{core}}/R_{\text{total}}$ is fixed to 0.857. From Figures 4, A and 4, B, it is evident that λ_{max} can be readily tuned throughout the NIR by varying the $R_{\text{core}}/R_{\text{total}}$ ratio or R_{total} . Extinction cross-sections at λ_{max} of the calculated structures are shown in Figures 4, C and 4, D. By increasing the core volume relative to the shell volume, a decrease of the $C_{\text{extinction}}$ is observed. The explanation is that gold is the dominant contributor to the $C_{\text{extinction}}$ at λ_{max} and that a smaller fraction of the total volume is gold in structures with a large $R_{\text{core}}/R_{\text{total}}$ ratio. If the $R_{\text{core}}/R_{\text{total}}$ is kept constant, an increase in the total size results in a larger $C_{\text{extinction}}$ at λ_{max} . The explanation is that the increase in total size augments the amount of material present in a single nanostructure, enhancing $C_{\text{extinction}}$. The $C_{\text{scattering}}/C_{\text{absorption}}$ at λ_{max} for the studied structures are shown in Figures 4, E and 4, F. It can be seen that increasing the $R_{\text{core}}/R_{\text{total}}$ ratio causes a decrease in $C_{\text{scattering}}/C_{\text{absorption}}$ at λ_{max} whereas an increase in R_{total} induces an increase for the same ratio. As stated in the general considerations earlier, the observed trends can be explained by contributions from Rayleigh scattering and the dielectric functions of the constituting materials. The findings presented here are consistent with the general considerations about plasmonic shells described earlier and show great similarities with the results for silica-gold core-shell NPs calculated by Jain et al.¹⁵

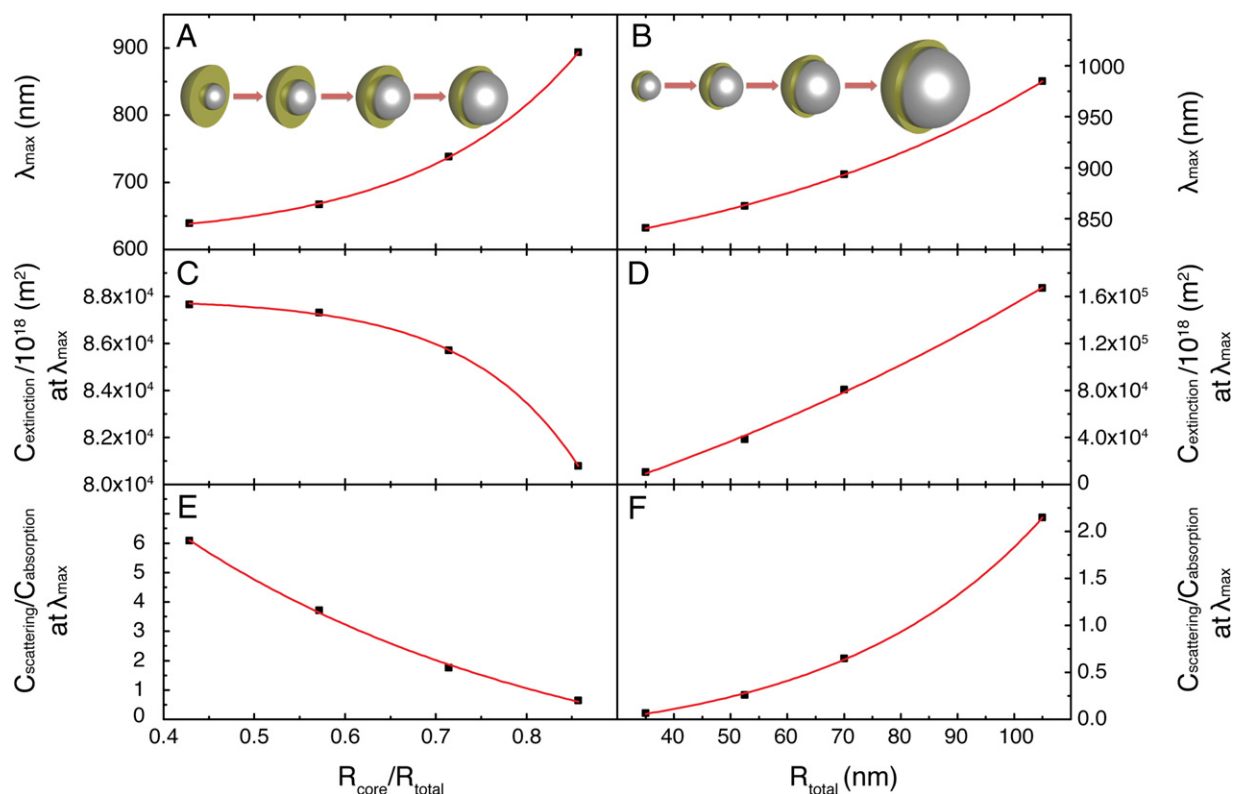


Figure 4. Dependencies of λ_{\max} , $C_{\text{extinction}}$ and the $C_{\text{scattering}}/C_{\text{absorption}}$ ratio at λ_{\max} on the $R_{\text{core}}/R_{\text{total}}$ ratio and R_{total} .

As stated earlier, to our knowledge no magnetic-plasmonic magnetite-gold core-shell nanospheres with a magnetite core as large as those used in our calculations have been synthesized. Nevertheless, the presented results show clear trends for all calculated properties and provide insight in the optical mechanisms at hand.

Magnetic-plasmonic nanorods

As stated earlier, core-shell nanorods can be described by three structural parameters: effective radius, aspect ratio, and $V_{\text{core}}/V_{\text{total}}$ ratio. During DDA calculations, each parameter was subsequently varied, and the two others remained constant. As such, calculations were performed for three different sets of core-shell magnetite-gold nanorods.

The first set consisted of nanorods with a fixed $R_{\text{effective}} = 10$ nm, a fixed aspect ratio of 3 (dimensions: 12x36 nm) and a $V_{\text{core}}/V_{\text{total}}$ ratio varying from 0 to 1. A second set of calculations involved structures with a fixed volume of $R_{\text{effective}} = 10$ nm, a fixed $V_{\text{core}}/V_{\text{total}}$ ratio of 0.2, and a varying aspect ratio from 1 (sphere) to 5. The calculation for the spherical structure in this series used Mie theory. For the last set of calculations a fixed $V_{\text{core}}/V_{\text{total}}$ ratio of 0.2, a fixed aspect ratio of 3 and a varying $R_{\text{effective}}$ of 5, 10, 15, or 20 nm were used. Combined results of these three sets of calculations allowed investigation of the influence of each of the three parameters ($V_{\text{core}}/V_{\text{total}}$, aspect ratio and $R_{\text{effective}}$) on the optical properties of the core-shell nanorods.

The resulting $Q_{\text{extinction}}$ of the aforementioned calculations are shown in Figures 5, A–C. As is evident from Figure 5, A, an increase in the $V_{\text{core}}/V_{\text{total}}$ ratio causes a redshift. This can be explained in the same way as it is for the core-shell nanospheres: By increasing the $V_{\text{core}}/V_{\text{total}}$ ratio, the gold shell surrounding the core becomes thinner, which facilitates the coupling of plasmonic modes across the shell, resulting in a redshift. It can also be seen from the same figure that a decrease in absolute $Q_{\text{extinction}}$ is observed for an increasing $V_{\text{core}}/V_{\text{total}}$ ratio. This can be explained by the fact that with increasing $V_{\text{core}}/V_{\text{total}}$ ratio, the contribution of gold decreases.

Figure 5, B shows the results of calculations on nanorods with different aspect ratios. Redshifts of the longitudinal dipolar plasmon resonance can be observed with increasing nanorod aspect ratio, accompanied by an increase in absolute $Q_{\text{extinction}}$. This is consistent with the explanation earlier; increasing aspect ratio increases the path length for electron oscillation along the long axis, causing redshifts.

It can be learned from Figure 5, C that increasing the volume of a nanorod with all other parameters unchanged leads to modest redshifts and an increase of $Q_{\text{extinction}}$. As for core-shell nanospheres, the explanation for this phenomenon is that the increase in total size augments the amount of material present in a single nanostructure, enhancing $C_{\text{extinction}}$. Obtained results are graphically summarized per variable parameter in Figure 6.

As shown in Figures 6, A–C, λ_{\max} can be tuned throughout the NIR by changing the composition, shape, or size of the nanorods. Figure 6, C shows that changing the $R_{\text{effective}}$ has only a modest effect on λ_{\max} because the redshift with augmenting

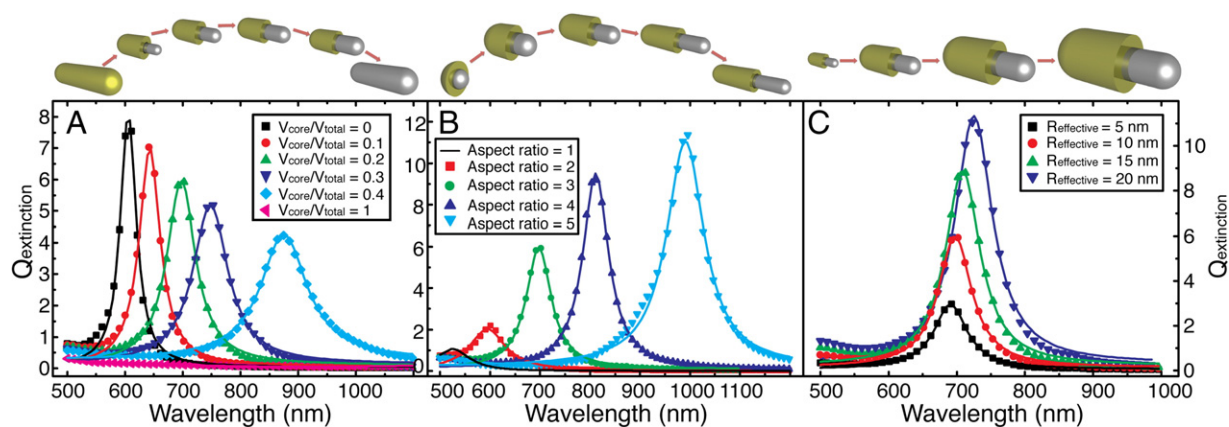


Figure 5. Calculated optical spectra of the $Q_{\text{extinction}}$ for three different sets of nanorods. (A) Fixed aspect ratio = 3, fixed $R_{\text{effective}} = 10$ nm, varying $V_{\text{core}}/V_{\text{total}}$ from 0 to 1; (B) Fixed $V_{\text{core}}/V_{\text{total}} = 0.2$, fixed $R_{\text{effective}} = 10$ nm, varying aspect ratio from 1 to 5; (C) Fixed $V_{\text{core}}/V_{\text{total}} = 0.2$, fixed aspect ratio = 3, varying $R_{\text{effective}} = 5, 10, 15$ and 20 nm. Note that the solid lines are fits to the data using Lorentzian curves. Spectra were calculated as the average response of two input polarizations, one in the plane of and one perpendicular to the long axis of the nanorods. Results show the redshift of λ_{max} and the changes in $Q_{\text{extinction}}$ when changing size, shape, or composition of the core-shell nanorods.

size is small in comparison with a change in aspect ratio or $V_{\text{core}}/V_{\text{total}}$ ratio. The extinction cross-section can be varied over a very broad range by changing one of the defining parameters, as can be observed in Figures 6, D–F. Although changing the $V_{\text{core}}/V_{\text{total}}$ ratio allows only modest tuning, varying the size of the structure provides the most efficient means for tuning $C_{\text{extinction}}$ at λ_{max} . As is evident from Figures 6, G–I, the range over which the $C_{\text{scattering}}/C_{\text{absorption}}$ ratio can be altered by changing the composition, shape, or size of the nanorods is quite narrow. As can be observed in Figure 6, I, the most effective way for tuning the $C_{\text{scattering}}/C_{\text{absorption}}$ ratio is altering the size, which can be explained by the size dependence of Rayleigh scattering.

The obtained results are consistent with the general considerations for core-shell nanorods. Magnetite nanorods with dimensions of 12 nm \times 48 nm, similar to the structure used in the calculations with an aspect ratio of 4 and $r_{\text{effective}}$ of 10 nm, have been chemically synthesized by Kumar et al.¹⁰ This demonstrates that the dimensions of the nanorod structures used in our calculations are realistic. Although pure iron oxide nanorods have been successfully synthesized,^{9,10} to our knowledge no magnetite-gold core-shell analog has been produced.

As with the core-shell nanospheres, the findings on magnetic-plasmonic nanorods can be used to select suitable particles for an envisioned application. For example, if a scattering imaging application is envisioned for which particles with a λ_{max} around 900 nm and a large $C_{\text{extinction}}$ are required, Figure 6 shows that particles with a large $V_{\text{core}}/V_{\text{total}}$ ratio, a high aspect ratio and a large $R_{\text{effective}}$ are best suited.

Quantitative comparison of magnetic-plasmonic nanospheres and nanorods

It is important to note that the trends observed for core-shell nanospheres and nanorods for similar parameters show great resemblance, as was expected from general considerations. Increasing the $R_{\text{core}}/R_{\text{total}}$ ratio for core-shell nanospheres or the

$V_{\text{core}}/V_{\text{total}}$ ratio for nanorods results in a redshifted λ_{max} , a decrease in the $C_{\text{extinction}}$ at λ_{max} , and a decrease in the $C_{\text{scattering}}/C_{\text{absorption}}$ ratio at λ_{max} . The same similarity was present for the size parameter. An increase in R_{total} for core-shell nanospheres or $R_{\text{effective}}$ for nanorods causes an increase in λ_{max} , the $C_{\text{extinction}}$ and the $C_{\text{scattering}}/C_{\text{absorption}}$ ratio at λ_{max} for both types of structures. These analogies arise because the same mechanisms operate in both structures.

Besides the similarity in the observed relative trends for the calculated structures, large absolute differences exist between the core-shell nanospheres and nanorod structures when properties per unit of volume are calculated. The results of these calculations are summarized in Table 1. For the calculations, we compare core-shell nanospheres with an R_{total} of 70 nm and a core-shell nanorod with a $R_{\text{effective}}$ of 10 nm and an aspect ratio of 3. Both studied structures have a $V_{\text{core}}/V_{\text{total}}$ ratio of 0.2.

The first calculated parameter is the shift of λ_{max} on a per volume basis. This shift is three orders of magnitude larger per unit of volume for the magnetic-plasmonic nanorods with aspect ratio 3 than for the nanospheres. A second assessed parameter is the $C_{\text{extinction}}$ per unit of volume at λ_{max} . An order of magnitude larger $C_{\text{extinction}}/\text{nm}^3$ at λ_{max} is calculated for the magnetic-plasmonic nanorod with aspect ratio 3 than for the core-shell spherical structure. From these results we can learn that although, theoretically, both core-shell nanospheres and nanorods can be tuned to have the same optical properties, these will be achieved at much smaller and more realistic volumes for core-shell nanorods.

Quantitative comparison of magnetic-plasmonic nanostructures and organic dyes

Organic dyes are frequently used in optical applications in the life sciences. To assess the applicability of the calculated magnetic-plasmonic nanostructures, we compared them with popular organic dyes. This comparison is only possible based on

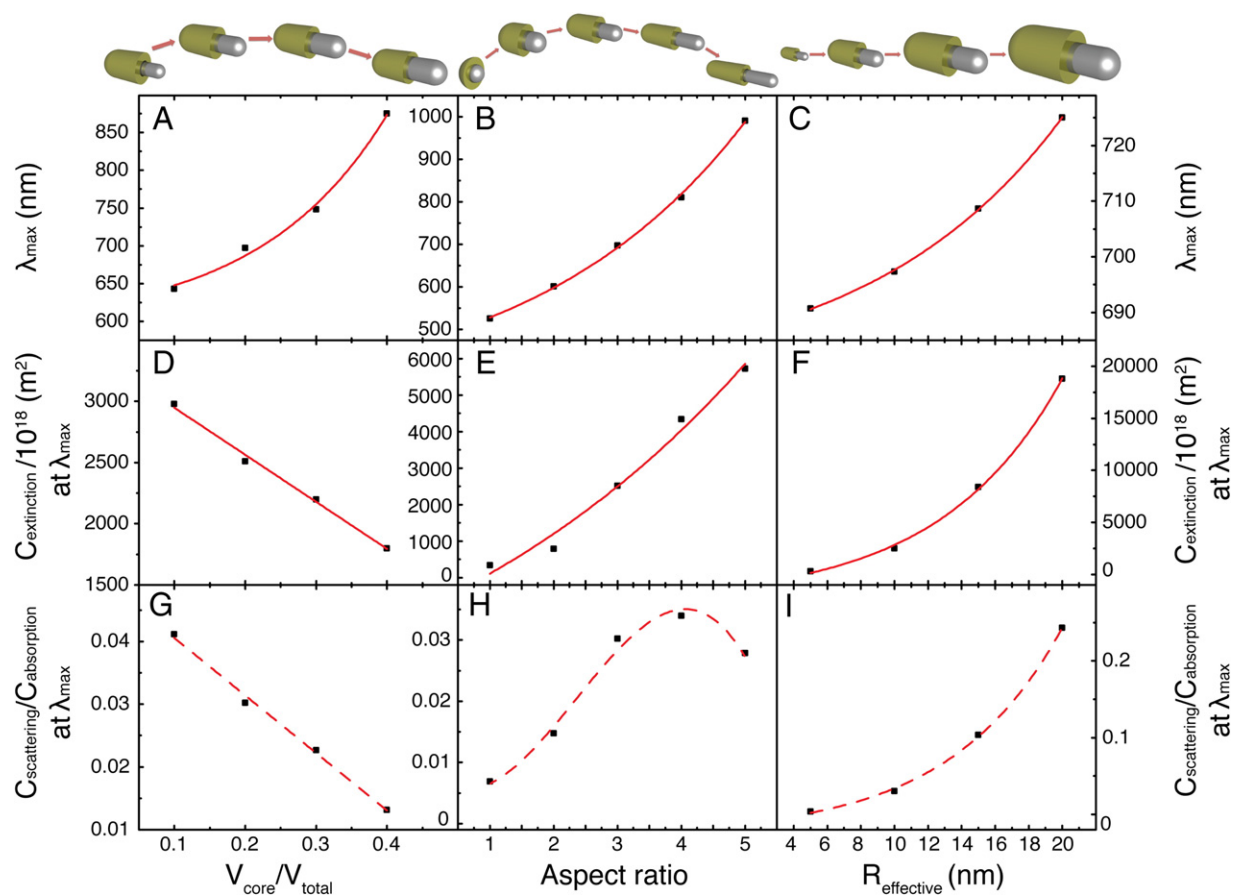


Figure 6. Dependencies of λ_{\max} , $C_{\text{extinction}}$ and the $C_{\text{scattering}}/C_{\text{absorption}}$ ratio at λ_{\max} on the $V_{\text{core}}/V_{\text{total}}$ ratio, the aspect ratio and $R_{\text{effective}}$.

Table 1
Values for parameters calculated on a per-volume basis for a core-shell nanosphere and a core-shell nanorod (aspect ratio 3) with the same $V_{\text{core}}/V_{\text{total}}$ ratio

Core-shell nanosphere			Core-shell nanorod		
Parameter	Value	Unit	Parameter	Value	Unit
R_{total}	70	Nm	$R_{\text{effective}}$	10	nm
V_{total}	1.4×10^6	nm^3	V_{total}	4189	nm^3
$V_{\text{core}}/V_{\text{total}}$	0.2		$V_{\text{core}}/V_{\text{total}}$	0.2	
Aspect ratio	1		Aspect ratio	3	
$\Delta\lambda_{\max}$	48	nm	$\Delta\lambda_{\max}$	86	nm
$\Delta\lambda_{\max}/\text{nm}^3$	3.34×10^{-5}	nm / nm^3	$\Delta\lambda_{\max}/\text{nm}^3$	0.02	nm / nm^3
$C_{\text{extinction}}/\text{nm}^3$	0.061	$10^{-18} \text{ m}^2 / \text{nm}^3$	$C_{\text{extinction}}/\text{nm}^3$	0.60	$10^{-18} \text{ m}^2 / \text{nm}^3$

molar coefficients calculated from the cross-sections using Equation 1.

For example, for a core-shell nanorod with an $R_{\text{effective}}$ of 10 nm, a $V_{\text{core}}/V_{\text{total}}$ ratio of 0.2, and an aspect ratio of 3, the molar coefficient of extinction, $\epsilon_{\text{extinction}}$, is $1.1 \times 10^{10} \text{ l.mol}^{-1}.\text{cm}^{-1}$ at the plasmon wavelength. Organic photosensitizers used for photodynamic therapy such as commercially available Photofrin ($\epsilon_{\text{extinction}} = 2.2 \times 10^4 \text{ l.mol}^{-1}.\text{cm}^{-1}$) or MACE ($\epsilon_{\text{extinction}} = 4.0 \times 10^4 \text{ l.mol}^{-1}.\text{cm}^{-1}$) or experimental phthalocyanines and naphthalocyanines ($\epsilon_{\text{extinction}} = 1.0 \times 10^5 \text{ l.mol}^{-1}.\text{cm}^{-1}$) or organic dyes such as heptamethine indocyanines

($\epsilon_{\text{extinction}} = 2 \times 10^5 \text{ l.mol}^{-1}.\text{cm}^{-1}$) show 5 to 6 orders of magnitude lower molar coefficients than plasmonic inorganic NPs do.^{24,48} Organic fluorescent molecules used for cellular imaging, such as Fluorescein⁴⁹ ($\epsilon = 9.2 \times 10^4 \text{ l.mol}^{-1}.\text{cm}^{-1}$ at 482.5 nm) or BODIPY dyes⁵⁰ ($\epsilon = 5.0 \times 10^4 \text{ l.mol}^{-1}.\text{cm}^{-1}$ at 512 nm), exhibit molar coefficients at emission wavelengths that are 3 to 4 orders of magnitude smaller than for the core-shell nanorod referred to above ($\epsilon_{\text{scattering}} = 1.9 \times 10^8 \text{ l.mol}^{-1}.\text{cm}^{-1}$ at 697 nm). In comparison with popular organic dyes, magnetite-gold nanostructures can possess higher molar coefficients, showing the applicability of such structures.

Discussion

Using Mie theory and DDA, optical properties of magnetic-plasmonic magnetite-gold nanospheres and nanorods were calculated. The influences of structural parameters as composition, size, and shape were investigated. From the results, we found that optical properties, such as λ_{\max} , the $C_{\text{extinction}}$, and the $C_{\text{scattering}}/C_{\text{absorption}}$ ratio at λ_{\max} of both core-shell nanospheres and nanorods, can be tuned by varying the structural parameters. It was calculated that magnetic-plasmonic nanospheres, which can be produced by available chemical synthetic methods, cannot provide efficient tuning of λ_{\max} throughout the NIR, nor the desired extinction efficiencies, and they are not suited for scattering applications due to a negligible $C_{\text{scattering}}/C_{\text{absorption}}$ ratio at λ_{\max} . On the other hand, core-shell nanorods show much larger values for the $C_{\text{extinction}}$ and the λ_{\max} shift on a per volume basis than core-shell nanospheres. Furthermore, magnetic-plasmonic nanorods show orders of magnitude larger molar extinction and scattering coefficients than organic materials used in current cancer treatment. With this knowledge it is possible to design and synthesize structures that possess a plasmon band in the advantageous NIR and other optical properties as desired for a potential application in life sciences.

Acknowledgments

The authors would like to thank M. Bloemen, M. Vanbel and S. Vandendriessche for useful discussions and critical reading of the manuscript.

References

- Bhattacharyya S, Kudgus RA, Bhattacharya R, Mukherjee P. Inorganic nanoparticles in cancer therapy. *Pharm Res* 2011;28:237-59.
- Liao Z, Wang H, Lv R, Zhao P, Sun X, Wang S, et al. Polymeric liposomes-coated superparamagnetic iron oxide nanoparticles as contrast agent for targeted magnetic resonance imaging of cancer cells. *Langmuir* 2011;27:3100-5.
- Kappiyoor R, Liangruksa M, Ganguly R, Puri IK. The effects of magnetic nanoparticle properties on magnetic fluid hyperthermia. *J Appl Phys* 2010;108:094702.
- Cobley CM, Chen J, Cho EC, Wang LV, Xia Y. Gold nanostructures: a class of multifunctional materials for biomedical applications. *Chem Soc Rev* 2011;40:44-56.
- Xie J, Lee S, Chen X. Nanoparticle-based theranostic agents. *Adv Drug Delivery Rev* 2010;62:1064-79.
- Cullity B, Graham C. Introduction to magnetic materials. 2nd ed. New Jersey: John Wiley & Sons, Inc.; 2009.
- Tartaj P, del Puerto Morales M, Veintemillas-Verdaguer S, Gonzalez-Carreno T, Serna CJ. The preparation of magnetic nanoparticles for applications in biomedicine. *J Phys D Appl Phys* 2003;36:182-97.
- Andrés Vergés M, Costo R, Roca AG, Marco JF, Goya GF, Serna CJ, et al. Uniform and water stable magnetite nanoparticles with diameters around the monodomain-multidomain limit. *J Phys D Appl Phys* 2008;41:134003.
- Chen S, Feng J, Guo X, Hong J, Ding W. One-step wet chemistry for preparation of magnetite nanorods. *Mater Lett* 2005;59:985-8.
- Kumar RV, Koltypin Y, Xu XN, Yeshurun Y, Gedanken A, Felner I. Fabrication of magnetite nanorods by ultrasound irradiation. *J Appl Phys* 2001;89:6324.
- Bergemann C, Mueller-Schulte D, Oster J, Brassard LA, Luebke AS. Magnetic ion-exchange nano- and microparticles for medical, biochemical and molecular biological applications. *J Magn Magn Mater* 1999;19445-52.
- Alexiou C, Tietze R, Schreiber E, Jurgons R, Richter H, Trahms L, et al. Cancer therapy with drug loaded magnetic nanoparticles — magnetic drug targeting. *J Magn Magn Mater* 2010;323:1404-7.
- Wang Y, Ravindranath S. Separation and detection of multiple pathogens in a food matrix by magnetic SERS nanoprobos. *Anal Bioanal Chem* 2011;1271-8.
- Kelly KL, Coronado E, Zhao LL, Schatz GC. The optical properties of metal nanoparticles: the influence of size, shape, and dielectric environment. *J Phys Chem B* 2003;107:668-77.
- Jain PK, Lee KS, El-Sayed IH, El-Sayed MA. Calculated absorption and scattering properties of gold nanoparticles of different size, shape, and composition: applications in biological imaging and biomedicine. *J Phys Chem B* 2006;110:7238-48.
- Govorov AO, Richardson HH. Generating heat with metal nanoparticles. *Nano Today* 2007;2:30-8.
- Jain PK, Huang X, El-Sayed IH, El-Sayed MA. Review of some interesting surface plasmon resonance-enhanced properties of noble metal nanoparticles and their applications to biosystems. *Plasmonics* 2007;2:107-18.
- Letfullin RR, Iversen CB, George TF. Modeling nanophotothermal therapy: kinetics of thermal ablation of healthy and cancerous cell organelles and gold nanoparticles. *Nanomed-Nanotechnol* 2011;7:137-45.
- Serksen S, Westcott S, Halas N, West J. Temperature-sensitive polymer-nanoshell composites for photothermally modulated drug delivery. *J Biomed Mater Res* 2000;51:293-8.
- Agarwal A, Huang SW, O'Donnell M, Day KC, Day M, Kotov N, et al. Targeted gold nanorod contrast agent for prostate cancer detection by photoacoustic imaging. *J Appl Phys* 2007;102:064701.
- Li Y, Schluesener HJ, Xu S. Gold nanoparticle-based biosensors. *Gold Bull* 2010;43:29-41.
- Tong L, Wei Q, Wei A, Cheng JX. Gold nanorods as contrast agents for biological imaging: optical properties, surface conjugation and photothermal effects. *Photochem Photobiol* 2009;85:21-32.
- Weissleder R. A clearer vision for in vivo imaging. *Nat Biotechnol* 2001;19:316-7.
- Frangioni J. In vivo near-infrared fluorescence imaging. *Curr Opin in Chem Biol* 2003;7:626-34.
- Rai P, Mallidi S, Zheng X, Rahmzadeh R, Mir Y, Elrington S, et al. Development and applications of photo-triggered theranostic agents. *Adv Drug Delivery Rev* 2010;62:1094-124.
- Chen W, Xu N, Xu L, Wang L, Li Z, Ma W, et al. Multifunctional magnetic-plasmonic nanoparticle assemblies for cancer therapy and diagnostics (theranostics). *Macromol Rapid Comm* 2010;31:228-36.
- Lee KS, El-Sayed M. a. Dependence of the enhanced optical scattering efficiency relative to that of absorption for gold metal nanorods on aspect ratio, size, end-cap shape, and medium refractive index. *J Phys Chem B* 2005;109:20331-8.
- Prodan E, Radloff C, Halas NJ, Nordlander P. A hybridization model for the plasmon response of complex nanostructures. *Science* 2003;302:419-22.
- Lu JY, Chiu KP, Chao HY, Chang YH. Multiple metallic-shell nanocylinders for surface-enhanced spectroscopies. *Nanoscale Res Lett* 2011;6:173.
- Brinson BE, Lassiter JB, Levin CS, Bardhan R, Mirin N, Halas NJ. Nanoshells made easy: improving Au layer growth on nanoparticle surfaces. *Langmuir* 2008;24:14166-71.
- Robinson I, Tung LD, Maenosono S, Wälti C, Thanh NTK. Synthesis of core-shell gold coated magnetic nanoparticles and their interaction with thiolated DNA. *Nanoscale* 2010;2:2624-30.

32. Hienpham T, Cao C, Sim S. Application of citrate-stabilized gold-coated ferric oxide composite nanoparticles for biological separations. *J Magn Magn Mater* 2008;320:2049-55.
33. Jain PK, Xiao Y, Walsworth R, Cohen AE. Surface plasmon resonance enhanced magneto-optics (SuPREMO): Faraday rotation enhancement in gold-coated iron oxide nanocrystals. *Nano Lett* 2009; 9:1644-50.
34. Lyon JL, Fleming DA, Stone MB, Schiffer P, Williams ME. Synthesis of Fe oxide core/Au shell nanoparticles by iterative hydroxylamine seeding. *Nano Lett* 2004;4:719-23.
35. Lim J, Eggeman A, Lanni F, Tilton RD, Majetich SA. Synthesis and single-particle optical detection of low-polydispersity plasmonic-superparamagnetic nanoparticles. *Adv Mater* 2008;20:1721-6.
36. Gonzalez-Diaz JB, Garcia-Martin A, Garcia-Martin JM, Cebollada A, Armelles G, Sepúlveda B, et al. Plasmonic Au/Co/au nano-sandwiches with enhanced magneto-optical activity. *Small* 2008; 4:202-5.
37. Wang L, Clavero C, Huba Z, Carroll KJ, Carpenter EE, Gu D, et al. Plasmonics and enhanced magneto-optics in core-shell Co-Ag nanoparticles. *Nano Lett* 2011;11:1237-40.
38. Albaladejo S, Gómez-Medina R, Froufe-Pérez LS, Marinchio H, Carminati R, Torrado JF. et. al. Radiative corrections to the polarizability tensor of an electrically small anisotropic dielectric particle. *Opt Express* 2010;18:3556-67.
39. Peña-Rodríguez O, González Pérez PP, Pal U. MieLab: A software tool to perform calculations on the scattering of electromagnetic waves by multilayered spheres. *Int J Sp* 2011;2011:583743.
40. Moreno E, Emi D, Hafner C, Vahldieck R. Multiple multipole method with automatic multipole setting applied to the simulation of surface plasmons in metallic nanostructures. *J Opt Soc Am A* 2002; 19:101-11.
41. Johnson P, Christy R. Optical constants of the noble metals. *Physical Review B* 1972;6:4370-9.
42. Goossens V, Wielant J, Van Gils S, Finsy R, Terryn H. Optical properties of thin iron oxide films on steel. *Surf Interface Anal* 2006: 38489-93.
43. Link S, El-Sayed MA. Size and temperature dependence of the plasmon absorption of colloidal gold nanoparticles. *J Phys Chem B* 1999;103: 4212-7.
44. Draine BT, Flatau PJ. Discrete-dipole approximation for scattering calculations. *J Opt Soc Am A* 1994;11:1491.
45. Draine BT, Flatau PJ. User guide to the discrete dipole approximation code DDSCAT 7.1. Available at: <http://arXiv.org/abs/1002.1505v1>. Accessed 2010.
46. Lakowicz JR. Principles of fluorescence spectroscopy, 6th ed. Springer; 2006. p. 59.
47. Hooshmand N, Jain P. Plasmonic spheroidal metal nanoshells showing larger tunability and stronger near fields than their spherical counterparts: an effect of enhanced plasmon coupling. *J Phys Chem Lett* 2011: 2374-8.
48. Prasad PN. Introduction to biophotonics. Hoboken, NJ: John Wiley & Sons, Inc; 2003.
49. Du H, Fuh R-chun A, Li J, Corkan LA, Lindsey JS. Technical and software note photochemcad: a computer-aided design and research tool in photochemistry. *Photochem Photobiol* 1998;68:141-2.
50. Schmitt A, Hinkeldey B, Wild M, Jung G. Synthesis of the core compound of the BODIPY dye class: 4,4'-difluoro-4-bora-(3a,4a)-diazas-indacene. *J Fluoresc* 2009;19:755-8.